

# Electrical transport and resistance switching characteristics of BiFeO<sub>3</sub>/Nb:SrTiO<sub>3</sub>/GaAs heterostructure fabricated by pulsed laser deposition

Cite as: Appl. Phys. Lett. **105**, 062904 (2014); <https://doi.org/10.1063/1.4890115>  
 Submitted: 06 May 2014 . Accepted: 01 July 2014 . Published Online: 13 August 2014

W. Huang, J. J. Yang, G. Y. Gao, Y. Lei, J. Zhu, H. Z. Zeng, F. G. Zheng, and J. H. Hao



View Online



Export Citation



CrossMark

## ARTICLES YOU MAY BE INTERESTED IN

[Temperature-dependent and polarization-tuned resistive switching in Au/BiFeO<sub>3</sub>/SrRuO<sub>3</sub> junctions](#)

Applied Physics Letters **104**, 143503 (2014); <https://doi.org/10.1063/1.4870813>

[Ferroelectric memristor based on Pt/BiFeO<sub>3</sub>/Nb-doped SrTiO<sub>3</sub> heterostructure](#)

Applied Physics Letters **102**, 102901 (2013); <https://doi.org/10.1063/1.4795145>

[Switchable diode effect and ferroelectric resistive switching in epitaxial BiFeO<sub>3</sub> thin films](#)

Applied Physics Letters **98**, 192901 (2011); <https://doi.org/10.1063/1.3589814>

Lock-in Amplifiers  
 Find out more today



Zurich  
 Instruments

## Electrical transport and resistance switching characteristics of BiFeO<sub>3</sub>/Nb:SrTiO<sub>3</sub>/GaAs heterostructure fabricated by pulsed laser deposition

W. Huang,<sup>1,2,a)</sup> J. J. Yang,<sup>1</sup> G. Y. Gao,<sup>3</sup> Y. Lei,<sup>1</sup> J. Zhu,<sup>1</sup> H. Z. Zeng,<sup>1,a)</sup> F. G. Zheng,<sup>2</sup> and J. H. Hao<sup>4</sup>

<sup>1</sup>State Key Laboratory of Electronic Thin Films and Integrated Devices, University of Electronics Science and Technology of China, Chengdu, People's Republic of China

<sup>2</sup>Jiangsu Key Laboratory of Thin Films, Soochow University, Suzhou 215006, People's Republic of China

<sup>3</sup>Hefei National Laboratory for Physical Sciences at Microscale, University of Science and Technology of China, Hefei, Anhui 230026, People's Republic of China

<sup>4</sup>Department of Applied Physics, The Hong Kong Polytechnic University, Hong Kong, People's Republic of China

(Received 6 May 2014; accepted 1 July 2014; published online 13 August 2014)

BiFeO<sub>3</sub> thin films were epitaxially grown on (001) GaAs substrate by pulsed laser deposition with Nb doped SrTiO<sub>3</sub> as a buffer layer. Piezoresponse force microscopy images exhibit effective ferroelectric switching of the heterostructure. The temperature-dependent current-voltage characteristics of the heterostructure reveal a resistance switching phenomenon and diode-like behavior with a rectifying ratio of  $2 \times 10^2$  at the applied voltage of  $\pm 13.4$  V. The electrical transport mechanism in the heterostructure has been illustrated by constructing the energy band structure. In addition, the resistance switching behavior in the heterostructure could be explained by the polarization modulation of the depletion region at the interface of the semiconductor and the ferroelectric layers.

© 2014 AIP Publishing LLC. [<http://dx.doi.org/10.1063/1.4890115>]

The heterostructures consisting of multiferroic BiFeO<sub>3</sub>(BFO) thin film have received noticeable attention because of their remarkable multiferroic and optical properties at room temperature.<sup>1–4</sup> Especially, the resistance of these BFO based heterostructures can be reversibly switched between a high resistance state (HRS) and a low resistance state (LRS) by applying voltages, which indicates the potential application of BFO based heterostructures in bistable memory devices.<sup>5,6</sup> The observed phenomena of resistive switching existed in BFO based heterostructures appear to vary with the processing conditions and microstructures of the BFO films, suggesting that several conduction mechanisms may be involved.<sup>7–11</sup> Previous studies mostly reported the electrical transport properties of BFO related thin films on various substrates. Wang *et al.* observed resistive switching behavior of SrRuO<sub>3</sub>(SRO)/BFO/Pt junctions, which could be modulated by the ferroelectric polarization. It was found that the ferroelectric polarization is capable of inducing blocking or non-blocking interfaces for the transport of electrical carriers, and consequently the observed switching behavior.<sup>12</sup> Tsurumaki-Fukuchi *et al.* has analyzed the carrier transport behavior in SRO/Bi<sub>1– $\delta$</sub> FeO<sub>3</sub>/SRO structure and a large number of screening charge separating from the polarization charge could be detected at the interface between the conducting SRO and ferroelectric BFO layer, which might be involved in the progress of the resistive switching behavior.<sup>13</sup> The electrical transport property in these structures is thought to be strongly dependent on the polarization modulation of energy band, but it is still not fully understood. Therefore, detailed knowledge of the

charge carrier dynamics is crucial for the realization of further application of these BFO heterostructures.

For practical application, the direct growth of the BFO on commonly used semiconductors, such as Si and GaAs, GaN has drawn much attention. As the lattice mismatch and growth environment incompatible, the epitaxial growth of BFO directly on semiconductor is still a challenge. Therefore, a buffer layer was usually engaged to realize epitaxial growth of these structures. For instance, Luo *et al.* realize the epitaxial growth of BFO films on GaN substrate using SrTiO<sub>3</sub>(STO)/TiO<sub>2</sub> double-layer buffer layer.<sup>14</sup> Yang *et al.* has grown BFO on GaN substrate using STO as buffer layer and studied the carriers transport characteristics of BFO/STO/GaN heteroepitaxial structures.<sup>15</sup> Among these semiconductors, GaAs should play an important role as a typical III–V semiconductor because of its direct band gap and higher saturated electron mobility. Recently, high-quality ferroelectric BaTiO<sub>3</sub> thin films with similar crystal structure of BFO have been deposited on GaAs by MBE and laser MBE techniques, which pave the way for the subsequent epitaxial growth of BFO on GaAs.<sup>16,17</sup> In our previous study, the epitaxial growth behavior of Mn-doped BFO grown on GaAs (001) with a Nb doped SrTiO<sub>3</sub> (NSTO) buffer layer has been reported, and the multiferroic properties of the heterostructure have been investigated.<sup>18</sup> In this work, the electrical transport property of BFO/NSTO/p-GaAs heterostructure was investigated by temperature dependent *I*-*V* characteristics. Resistive switching phenomenon was discussed according to the band structure of the heterostructure combined with ferroelectric polarization in BFO film.

The BFO films were grown on the p-type GaAs (001) substrate by pulsed laser deposition (PLD) using an excimer laser ( $\lambda = 248$  nm) via a 100 nm thick NSTO (001) thin film as buffer layer. The conductive NSTO buffer layer could be

<sup>a)</sup>Authors to whom correspondence should be addressed. Electronic addresses: uestchw@uestc.edu.cn and zenghz@uestc.edu.cn

grown on p-GaAs (001) directly at 590 °C, the experimental details can be referred in our previous reports.<sup>17,19–21</sup> After the buffer layer deposition, the substrate temperature was fixed at 620–650 °C, and the oxygen pressure was raised up to 9 Pa for subsequent BFO deposition. During deposition, the laser frequency and energy density were kept at 10 Hz and 6 J/cm<sup>2</sup>, respectively. The distance between the target and substrate was 5 cm. The thickness of the BFO was about 300 nm. After BFO deposition, the sample was *in situ* annealed at 420 °C in 100 Pa of partial oxygen pressure before cooled down to room temperature in order to compensate oxygen vacancies in the films.<sup>22</sup> Finally, Pt electrode with a diameter of 0.2 mm was sputtered onto the BFO films as top electrode to form ohmic contact. The crystal structure of the samples was examined by X-ray diffraction (XRD) technique. The surface morphology and piezoelectric force microscopy (PFM) measurements were carried out on a scanning probe microscope (SPM). The cross-sectional morphology of the heterostructure was observed using a FEI FP2003/11 field emission scanning electron microscope, operated at an accelerating voltage of 20 kV. The measurement of *I-V* characters was performed by using a Keithley 2400 meter with the step voltage of 0.1 V. Pt electrodes were sputtered onto the BFO films and GaAs substrate as top and bottom electrode, respectively. The voltage was defined as “positive” when the bottom Pt electrode was grounded and “negative” when the top Pt electrode was grounded.

Figure 1 shows a typical  $\Theta$ - $2\Theta$  XRD scan curve on a semi-logarithmic scale for BFO films grown on Nb-STO buffered p-GaAs (001) substrate. Only (00 $l$ ) reflections from BFO films were observed besides the GaAs (00 $l$ ) reflections. Almost no second phase could be observed in the scan indicating that the films have a mostly single (00 $l$ ) orientation. According to Bragg’s diffraction law, STO unit began to grow with a 45° in-plane rotation on GaAs to get a comfortable lattice match due to a large mismatch between STO ( $a = 3.905 \text{ \AA}$ ) and GaAs ( $a = 5.65 \text{ \AA}$ ), which is consistent with the observation in Ref. 23. The lattice constant of the BFO film was calculated to be 3.959 Å, comparable to that of bulk BFO, indicating fully relaxed strain state in the films. Meanwhile, no Nb-STO peaks were observed in the scan because of the peaks of BFO films covered it and lower intensity of the peaks due to thinner

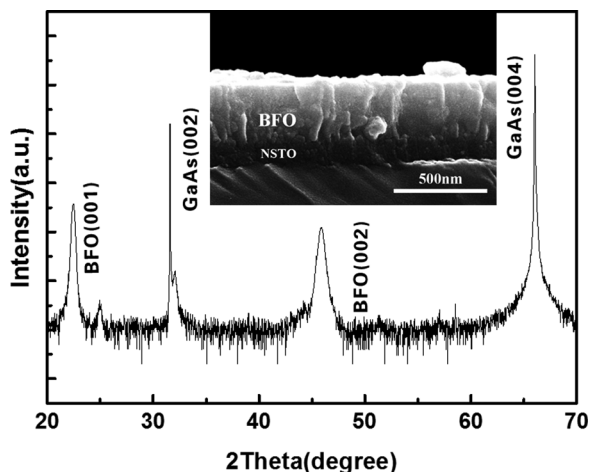


FIG. 1. XRD scan for the BFO films grown on NSTO buffered GaAs (001) substrate. The inset is cross-sectional scanning electron micrographs of the BFO/NSTO/GaAs heterojunction.

thickness of Nb-STO. The cross-sectional morphology of the heterostructure is shown in the inset of Figure 1. It can be seen that the BFO film has grown columnar on NSTO buffer layer with a clear interface.

To understand the influence of ferroelectric polarization on the electrical transport property of BFO/NSTO/p-GaAs heterostructure, SPM was performed to characterize the surface structure of the as-grown sample. Figure 2(a) shows the topography of the BFO film on GaAs (001) substrate with the area size of  $1.5 \times 1.5 \mu\text{m}^2$ . One can see that BFO surface is distributed with 3D islands randomly nucleated on the surface,<sup>24</sup> and the root mean square roughness of the surface is about 10 nm. The local ferroelectric properties of the heterostructure were examined by PFM. The amplitude and phase signals of vertical PFM (VPFM) were simultaneously obtained on the surface of the samples at same area, as shown in Figures 2(b) and 2(c), respectively. From these images, a color contrast corresponding to a poly-domain state can be clearly seen under the PFM measurement with an ac bias voltage of 2.5 V. The strong dark and bright contrast of the VPFM image (Fig. 2(b)) imply a large polarization perpendicular to the BFO film. Piezoelectric contrast can also be switched with a DC voltage applied to the tip. The out-of-plane polarization was reversed effectively when bias voltage switched from 30 V to  $-30 \text{ V}$  (Fig. 2(d)). Besides, a slight offset of the PFM hysteresis loop is observed, which could be attributed to the clamping effect from substrate. The PFM hysteresis loop from out-of-plane was investigated as a function of the applied electric field. In the measurement, the ac voltage was 1 V at 46 kHz. The measured coercive electric-voltage ( $V_c$ ) is about 16 V, indicating the ferroelectric behavior of spontaneous polarization in BFO films grown on GaAs at nanoscale.

Figure 3 shows the current-voltage (*I-V*) curves measured on the sample at the temperature ranging from 150 K to

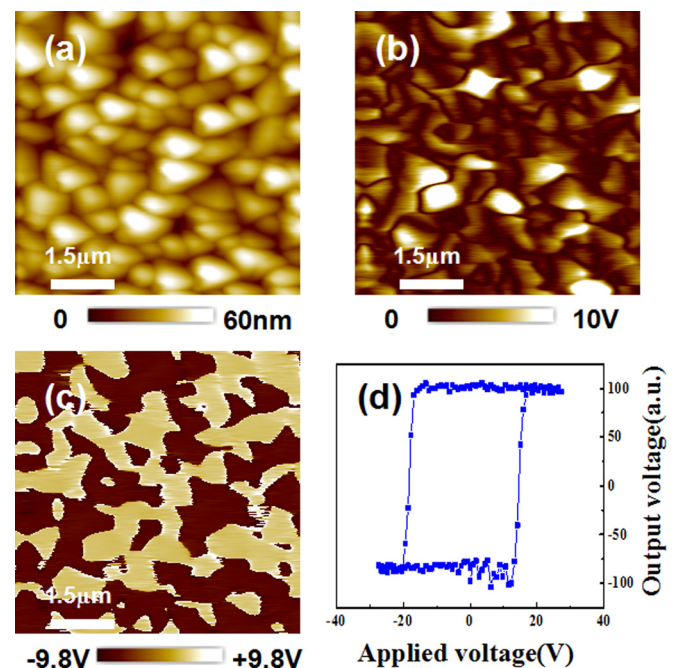


FIG. 2. (a) Surface morphology of the BFO/NSTO/GaAs heterostructure; (b) amplitude and (c) phase PFM images of the BFO/NSTO/GaAs heterostructure; (d) the piezoresponse output of the BFO/NSTO/GaAs heterostructure as a function of the applied electric voltage.

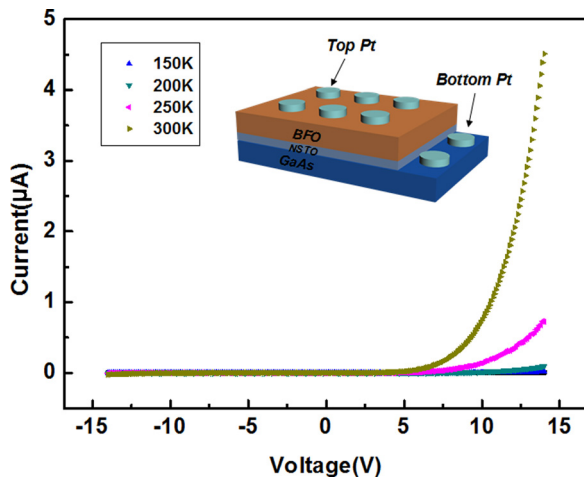


FIG. 3. I-V curves of BFO/NSTO/GaAs heterostructure from 150 K to 300 K. The inset shows the schematic of Pt/BFO/NSTO/GaAs heterostructure.

300 K, and the sweeping voltage is from  $-14$  V to  $14$  V. Here, the forward bias was defined as a positive voltage applied on top Pt electrode and negative voltage applied on p-GaAs. As seen in Fig. 3 in the BFO/NSTO/GaAs heterostructure, the I-V curves show typical diode-like current characteristics and the value of threshold voltage is about  $5$  V at room temperature. The rectifying ratio is about  $2 \times 10^2$  at the applied voltage of  $\pm 13.4$  V. At a given voltage, the current density decreases with the decreasing temperature. The similar results have been found in other heterostructures.<sup>25,26</sup> Compared with STO/GaAs structure,<sup>25</sup> the threshold voltage increased and it could be attributed to the band structure of as-grown BFO thin film on STO/GaAs.

In order to further investigate the electrical transport behavior of the BFO/NSTO/GaAs heterostructure, the energy band diagram is schematically illustrated in Fig. 4 in order to explain the current-voltage (I-V) characteristics. Generally, BFO films exhibit p-type conduction as a result of Bi loss.<sup>27–29</sup> For NSTO buffer layer, it is usually treated as n-type semiconductor with an energy band gap of  $3.2$  eV and an electron affinity of  $4$  eV.<sup>30,31</sup> Thus, a p-n junction can be formed at the BFO/n-type semiconductor interface. For Nb-STO, BFO, and GaAs, the values of electron affinity [ $\chi(\text{Nb-STO}) = 4.0$  eV,  $\chi(\text{BFO}) = 3.3$  eV,  $\chi(\text{GaAs}) = 4.1$  eV] and energy band gap [ $E_g(\text{Nb-STO}) = 3.2$  eV,  $E_g(\text{BFO}) = 2.8$  eV,  $E_g(\text{GaAs}) = 1.42$  eV] were taken to construct the band structure.<sup>25,30–32</sup> The band

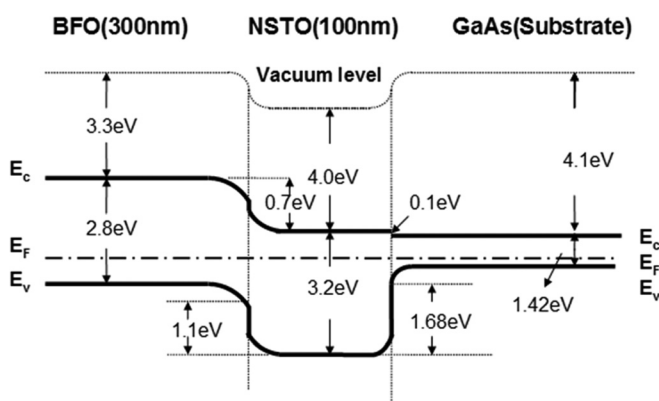


FIG. 4. Schematic energy band diagram of the BFO/NSTO/p-GaAs heterostructure.

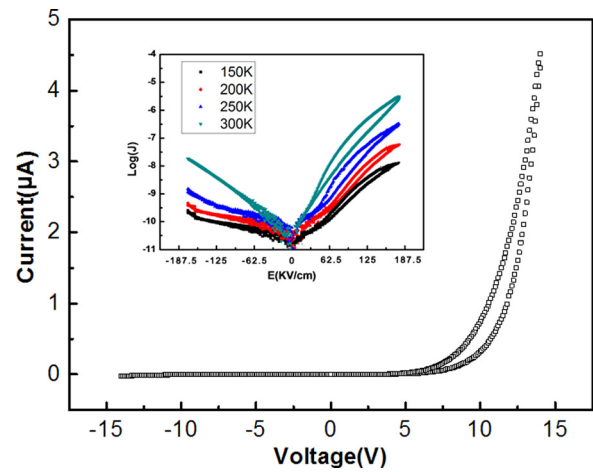


FIG. 5. I-V curves of BFO/NSTO/GaAs heterostructure at room temperature. The inset is  $\log(I)$  vs  $E$  at the experiment temperature from 150 K to 300 K, respectively.

offset value of the conduction band between BFO and NSTO is  $0.7$  eV [ $\Delta E_c = \chi(\text{Nb-STO}) - \chi(\text{BFO})$ ] and that of the valence band is  $1.1$  eV [ $\Delta E_v = [\chi(\text{Nb-STO}) - \chi(\text{BFO})] + [E_g(\text{Nb-STO}) - E_g(\text{BFO})]$ ]. In a similar way, the  $\Delta E_c$  and  $\Delta E_v$  of NSTO/GaAs could be calculated to be  $0.1$  eV [ $\Delta E_c = \chi(\text{GaAs}) - \chi(\text{Nb-STO})$ ] and  $1.68$  eV [ $\Delta E_v = [\chi(\text{Nb-STO}) - \chi(\text{GaAs})] + [E_g(\text{Nb-STO}) - E_g(\text{GaAs})]$ ], respectively. Accordingly, the parameters of the band structure are illustrated as seen in Fig. 4. Since the barrier height for holes is  $0.2$  eV larger than that for electrons, the hole current will be approximately a factor of  $10^4$  smaller than the electron current, suggesting that the current is dominated by the electrons in our heterostructure.<sup>33</sup> When the forward voltage was applied on the BFO/NSTO/GaAs heterostructure, the electrons would transfer from BFO to p-GaAs. When the negative voltage was applied on the BFO/NSTO/GaAs heterostructure, the energy barrier between BFO and NSTO would hinder the transport of electrons which results in a small current.<sup>25,28</sup> Moreover, based on the band structure, the heterostructure can be treated as two back to back PN junctions and exhibits diode-like I-V characters with increased threshold voltage.

Figure 5 shows a typical I-V curve of the heterostructure at room temperature, indicating resistive switching characteristic. The bias voltage was swept as  $-14 \rightarrow 0 \rightarrow +14 \rightarrow 0 \rightarrow -14$  V. It is apparent that the heterostructure exhibits a high resistance state when sweeping from  $0$  to  $+14$  V, and a low resistance state when sweeping from  $+14$  V to  $0$  V. The I-V measurements have been carried out in the temperature range of  $150$  K– $300$  K, as shown in the inset of Fig. 5. While the temperature decreases, the hysteresis (in logarithmic scale) window is getting smaller. As seen in Fig. 5, a resistive switching behavior could be obviously observed from the I-V curves. We have also measured hysteresis I-V characteristic for different bias voltage (not shown here). All I-V curves exhibit a similar hysteresis property. In previous studies, a diode-like rectifying I-V characteristic without the switching behavior has been observed in STO/GaAs and other oxide/GaAs related heterostructures.<sup>8,19</sup> As a consequence, we consider that the switching behavior in the BFO/NSTO/GaAs heterostructure could be attributed to the influence of BFO films. The similar electrical transport behavior has also been

reported in other systems of ferroelectric-semiconductor structures.<sup>9–11,34,35</sup> For instance, Voora explained these electron transport properties in BTO/ZnO heterojunction with depletion layer formation between the ferroelectric/semiconductor layers, which would result in the occurrence of an additional barrier at the interface between the BTO and ZnO due to the spontaneous polarization of the structures and therefore caused the resistive switching behavior.<sup>10,36</sup>

In our case, the observed resistive switching behavior in BFO/NSTO/GaAs heterostructure can be understood by the ferroelectric polarization modulation effect on the width of depletion region and then influence the height of potential barrier at the BFO/NSTO interface.<sup>37</sup> According to the energy band diagram as seen in Fig. 4, a depletion region with a certain width occurs at the BFO/NSTO interface and the depletion region would induce an energy band bending at the interface accordingly.<sup>38</sup> When the ferroelectric polarization in BFO is downward after applying positive voltage, the positive polarization bound charges aggregate at the BFO/NSTO interface. Meanwhile, the electron carriers in n-type NSTO are attracted by these positive bound charges and migrate toward the interface, resulting in a decrease of the depletion width. In other words, a decrease of the barrier height at the interface between BFO and NSTO.<sup>39</sup> In contrast, when the polarization is upward after applying a negative voltage, the electrons in n-type NSTO are repelled by the negative bound charges at the BFO/NSTO interface, and then increase the depletion width. As a result, the depletion regions and energy barrier heights in BFO/NSTO/GaAs heterostructure are changed and the resistance switching behavior occurs.

In conclusion, the BFO/NSTO/GaAs heterostructure has been fabricated by PLD. The temperature-dependent current-voltage characteristics of the heterostructure reveal a resistance switching phenomenon and diode-like behavior with a rectifying ratio of  $2 \times 10^2$  at the applied voltage of  $\pm 13.4$  V. Combined with the energy band structure, the electrical transport mechanism could be attributed to the ferroelectric polarization modulation effect on the width of depletion region and then influence the height of potential barrier at the BFO/NSTO interface.

The authors would like to thank Dr. H. C. He for technical support and useful discussion. The project was supported by Open Fund of IPOC (BUPT) Grant No. IPOC2013B006 and was also supported by grants from the Fundamental Research Funds for the Central Universities of China (Grant Nos. ZYGX2013J040 and ZYGX2012J032) and the National Natural Science Foundation of China (Grant Nos. 51272166 and 51002023).

<sup>1</sup>F. Gao, Y. Yuan, K. F. Wang, X. Y. Chen, F. Chen, J. M. Liu, and Z. F. Ren, *Appl. Phys. Lett.* **89**(10), 102506 (2006).

<sup>2</sup>X. D. Qi, J. Dho, R. Tomov, M. G. Blamire, and J. L. MacManus-Driscoll, *Appl. Phys. Lett.* **86**(6), 062903 (2005).

<sup>3</sup>R. Haumont, J. Kreisel, P. Bouvier, and F. Hippert, *Phys. Rev. B* **73**, 132101 (2006).

<sup>4</sup>H. Béa, M. Bibes, S. Fusil, K. Bouzehouane, E. Jacquet, K. Rode, P. Bencok, and A. Barthélémy, *Phys. Rev. B* **74**, 020101(R) (2006).

<sup>5</sup>S. Y. Yang, L. W. Martin, S. J. Byrnes, T. E. Conry, S. R. Basu, D. Paran, L. Reichertz, J. Ihlefeld, C. Adamo, A. Melville, Y. H. Chu, C. H. Yang, J. L. Musfeldt, D. G. Schlom, J. W. Ager, and R. Ramesh, *Appl. Phys. Lett.* **95**(6), 062909 (2009).

<sup>6</sup>T. Choi, S. Lee, Y. J. Choi, V. Kiryukhin, and S. W. Cheong, *Science* **324**(5923), 63 (2009).

<sup>7</sup>J. G. Wu and J. Wang, *J. Appl. Phys.* **108**(3), 034102 (2010).

<sup>8</sup>P. D. Ye, B. Yang, K. K. Ng, J. Bude, G. D. Wilk, S. Halder, and J. C. M. Hwang, *Appl. Phys. Lett.* **86**(6), 063501 (2005).

<sup>9</sup>J. G. Wu and J. Wang, *J. Appl. Phys.* **108**(9), 094107 (2010).

<sup>10</sup>V. M. Voora, T. Hofmann, M. Schubert, M. Brandt, M. Lorenz, M. Grundmann, N. Ashkenov, and M. Schubert, *Appl. Phys. Lett.* **94**(14), 142904 (2009).

<sup>11</sup>M. X. Zhou, Z. W. Li, B. Chen, J. G. Wan, and J. M. Liu, *J. Phys. D: Appl. Phys.* **46**(16), 165304 (2013).

<sup>12</sup>C. Wang, K. J. Jin, Z. T. Xu, L. Wang, C. Ge, H. B. Lu, H. Z. Guo, M. He, and G. Z. Yang, *Appl. Phys. Lett.* **98**(19), 192901 (2011).

<sup>13</sup>A. Tsurumaki-Fukuchi, H. Yamada, and A. Sawa, *Appl. Phys. Lett.* **103**(15), 152903 (2013).

<sup>14</sup>W. B. Luo, J. Zhu, H. Z. Zeng, X. W. Liao, H. Chen, W. L. Zhang, and Y. R. Li, *J. Appl. Phys.* **109**(10), 104108 (2011).

<sup>15</sup>S. Y. Yang, Q. Zhan, P. L. Yang, M. P. Cruz, Y. H. Chu, R. Ramesh, Y. R. Wu, J. Singh, W. Tian, and D. G. Schlom, *Appl. Phys. Lett.* **91**(2), 022909 (2007).

<sup>16</sup>R. Contreras-Guerrero, J. P. Veazey, J. Levy, and R. Droopad, *Appl. Phys. Lett.* **102**(1), 012907 (2013).

<sup>17</sup>W. Huang, Z. P. Wu, and J. H. Hao, *Appl. Phys. Lett.* **94**(3), 032905 (2009).

<sup>18</sup>G. Y. Gao, Z. B. Yang, W. Huang, H. Z. Zeng, Y. Wang, H. L. W. Chan, W. B. Wu, and J. H. Hao, *J. Appl. Phys.* **114**(9), 094106 (2013).

<sup>19</sup>Z. P. Wu, W. Huang, K. H. Wong, and J. H. Hao, *J. Appl. Phys.* **104**(5), 054103 (2008).

<sup>20</sup>W. Huang, J. Y. Dai, and J. H. Hao, *Appl. Phys. Lett.* **97**(16), 162905 (2010).

<sup>21</sup>Z. B. Yang, W. Huang, and J. H. Hao, *Appl. Phys. Lett.* **103**(3), 031919 (2013).

<sup>22</sup>H. Yang, M. Jain, N. A. Suvorova, H. Zhou, H. M. Luo, D. M. Feldmann, P. C. Dowden, R. F. DePaula, S. R. Foltyn, and Q. X. Jia, *Appl. Phys. Lett.* **91**(7), 072911 (2007).

<sup>23</sup>Y. Liang, J. Kulik, T. C. Eschrich, R. Droopad, Z. Yu, and P. Maniar, *Appl. Phys. Lett.* **85**(7), 1217 (2004).

<sup>24</sup>J. L. Li, J. H. Hao, Z. Ying, and Y. R. Li, *Appl. Phys. Lett.* **91**(20), 201919 (2007).

<sup>25</sup>X. H. Wei, W. Huang, Z. B. Yang, and J. H. Hao, *Scr. Mater.* **65**(4), 323 (2011).

<sup>26</sup>Q. X. Jia, B. Maiorov, H. Wang, Y. Lin, S. R. Foltyn, L. Civale, and J. L. MacManus-Driscoll, *IEEE Trans. Appl. Supercond.* **15**(2), 2723 (2005).

<sup>27</sup>A. Tsurumaki, H. Yamada, and A. Sawa, *Adv. Funct. Mater.* **22**(5), 1040 (2012).

<sup>28</sup>H. Yang, H. M. Luo, H. Wang, I. O. Sotov, N. A. Suvorova, M. Jain, D. M. Feldmann, P. C. Dowden, R. F. DePaula, and Q. X. Jia, *Appl. Phys. Lett.* **92**(10), 102113 (2008).

<sup>29</sup>D. Lee, S. H. Baek, T. H. Kim, J. G. Yoon, C. M. Folkman, C. B. Eom, and T. W. Noh, *Phys. Rev. B* **84**, 125305 (2011).

<sup>30</sup>Y. Watanabe, *Phys. Rev. B* **57**, R5563 (1998).

<sup>31</sup>S. M. Guo, Y. G. Zhao, C. M. Xiong, and P. L. Lang, *Appl. Phys. Lett.* **89**(22), 223506 (2006).

<sup>32</sup>S. J. Clark and J. Robertson, *Appl. Phys. Lett.* **90**(13), 132903 (2007).

<sup>33</sup>D. A. Neamen, *Semiconductor Physics and Devices: Basic Principles*, 3rd ed. (McGraw-Hill, New York, 2003), Vol. 9, pp. 350–359.

<sup>34</sup>Y. Lin, B. R. Zhao, H. B. Peng, Z. Hao, B. Xu, Z. X. Zhao, and J. S. Chen, *J. Appl. Phys.* **86**(8), 4467 (1999).

<sup>35</sup>J. S. Lee, Y. Li, Y. Lin, S. Y. Lee, and Q. X. Jia, *Appl. Phys. Lett.* **84**(19), 3825 (2004).

<sup>36</sup>V. M. Voora, T. Hofmann, M. Brandt, M. Lorenz, M. Grundmann, N. Ashkenov, H. Schmidt, N. Ianno, and M. Schubert, *Phys. Rev. B* **81**, 195307 (2010).

<sup>37</sup>R. Meyer and R. Waser, *J. Appl. Phys.* **100**(5), 051611 (2006).

<sup>38</sup>S. M. Sze and K. K. Ng, *Physics of Semiconductor Devices* (Wiley Interscience, Hoboken, 2007).

<sup>39</sup>Y. Watanabe, *Phys. Rev. B* **59**, 11257 (1999).